A Study on Deep Learning-Based Predictive Modeling of Vegetation Dynamics in Kazakhstan through the Integration of CNNs, RNNs, and Satellite Imagery for Ecological Monitoring

Aizhan Altaibek
International Information Technology University, Almaty, 05000, Kazakhstan | Institute of Ionosphere, Almaty, 050020, Kazakhstan
aizhan.altaibek@yandex.kz

Marat Nurtas
International Information Technology University, Almaty, 05000, Kazakhstan | Institute of Ionosphere, Almaty, 050020, Kazakhstan
maratnurtas@gmail.com (corresponding author)

Serik Nurakynov
Institute of Ionosphere, Almaty, 050020, Kazakhstan
snurakynov@ionos.kz

Aigerim Kaken
Institute of Ionosphere, Almaty, 050020, Kazakhstan
aigerim.kken03@gmail.com

Received: 31 March 2025 | Revised: 2 May 2025 | Accepted: 8 May 2025

 DOI: https://doi.org/10.48084/etasr.11188

ABSTRACT

The present study focused on applying deep learning methods to analyze the dynamics of vegetation in Kazakhstan's ecosystem. Satellite-based indices, such as Normalized Difference Vegetation Index (NDVI) and Enhanced Vegetation Index (EVI) were utilized to develop predictive models assessing the effects of environmental parameters on vegetation health. Convolutional Neural Networks (CNNs) were employed for spatial feature extraction along with Recurrent Neural Networks (RNNs) for capturing temporal dependencies. Initially, the ResNet-50 model was deployed with the results revealing a poor correlation with the actual vegetation patterns. Extensive preprocessing and optimization methods, such as batch normalization and gradient clipping, were applied, and the findings demonstrated a significant improvement in predictive precision, enabling accurate forecasts of vegetation changes. This work highlighted the potential of combining advanced technology with ecological research to develop solutions for managing climate impacts.

Keywords-vegetation dynamics; DL; NDVI; EVI; CNNs; RNNs; climate change; Kazakhstan

I. INTRODUCTION

As climate and human activity change, it is important to understand how vegetation responds in order to maintain biodiversity. Kazakhstan is a country with vast territories and ecological variety, ranging from semi-desert to the steppe zone, as well as mountains and forests. Steppes alone cover about 28% of the total land area with more than 6,000 plant types, 500 bird species, and 150 mammal kinds included in the country's ecosystem [1]. However, the stability of these habitats is constantly threatened by several biogenic and anthropogenic sources [2].

The Aral Sea desiccation, as depicted in Figure 1, was one of the most significant environmental disasters of the 20th century. Its surface area decreased from 58,000 km² to less than

8.000 km² in a time period of 37 years, revealing the progressive shrinkage of the sea. Particularly, the water volume declined by over 90% while the salinity increased from 10 g/L to more than 100 g/L, leading to the extinction of most fish species and consequently to the collapse of fishing industry [3]. Except these, the disaster impacted public health, including a rise in respiratory diseases, anemia, and cancer [4]. The consequences of current tendencies for the territory of Kazakhstan are associated with rising temperatures and changes in the precipitation regime (Figure 2), which enhance the process of desertification and further strain water resources [5].

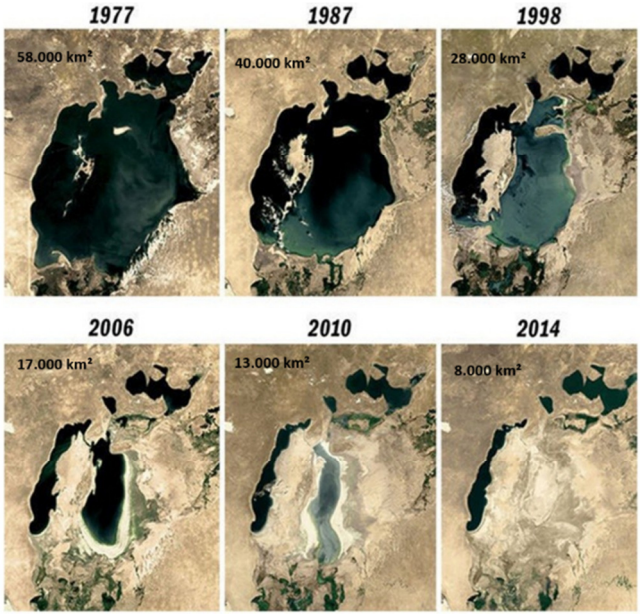

Fig. 1. Progressive desiccation of the Aral Sea (1977–2014).

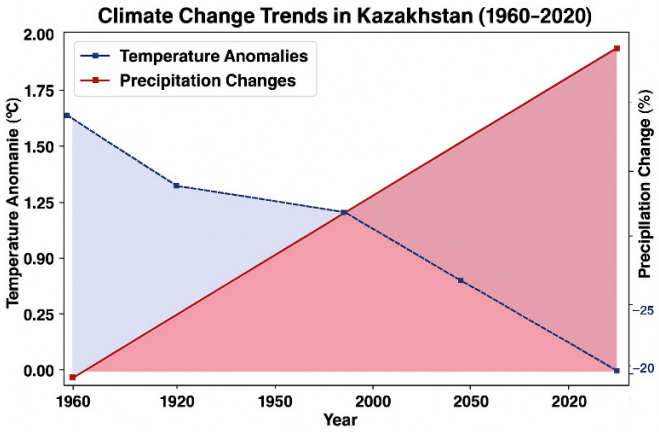

Fig. 2. Trends in temperature anomalies and precipitation changes in Kazakhstan (1960–2020).

For these reasons, the Government of Kazakhstan, in conjunction with many international organizations, has done several actions towards the conservation of its biodiversity by establishing nature reserves and national parks. In 2021, about ten national parks and a number of protected areas were established. Such strategies should be based on comprehensive environmental monitoring and management plans integrated with sustainable practices that align with global environmental norms.

To address these challenges, the present research applied deep learning techniques to forecast vegetation health and distribution using indices, such as NDVI and Enhanced EVI, as well as CNNs and Recurrent RNNs for the analysis of both spatial and temporal patterns [6].

II. DATA COLLECTION AND PREPROCESSING

A. Data Collection

A comprehensive dataset was constructed using Moderate Resolution Imaging Spectroradiometer (MODIS) products onboard NASA's Aqua and Terra satellites [7]. Specifically, the MOD13Q1 Vegetation Index product was utilized, which provided 16-day composites of the NDVI and EVI at a spatial resolution of 250 m. The dataset covered a period from 20 April 2022 to 1 September 2023, encompassing the entire territory of Kazakhstan (36.4212°–55.7177° N, 46.2508°–87.6306° E), thereby enabling detailed observation of seasonal and regional vegetation patterns.

To ensure temporal consistency, daily precipitation data from Advanced Microwave Scanning Radiometer 2 (AMSR2) and Special Sensor Microwave Imager onboard the Defense Meteorological Satellite Program (SSMI/DMSP) were aggregated into 16-day periods. This alignment combined with the NDVI composite interval facilitated time-synchronized analysis of vegetation response to rainfall. Additionally, precipitation rate maps from the Integrated Multi-Satellite Retrievals for GPM (IMERG) product were employed to enhance the dataset with high-resolution rainfall information. All imagery was retrieved using NASA's Worldview Snapshot API through automated scripts developed in Python, ensuring consistency and reducing manual errors.

B. Preprocessing

The preprocessing stage involved several steps to prepare the raw data for analysis. Initially, satellite images underwent cleaning through correction algorithms to remove artifacts, such as cloud cover and sensor noise. This was followed by reprojection to a common coordinate system and resampling to a unified spatial resolution. A min-max normalization method was applied to scale both vegetation indices and precipitation values to a [0, 1] range, preserving their relative distributions while ensuring compatibility for modeling. Precipitation data were also temporally aggregated to match the NDVI intervals. The processed dataset consisted of 499 preprocessed and temporally aligned NDVI-precipitation samples. Of those, 80% (399 samples) were used for model training, and 20% (100 samples) for validation [8].

C. Satellite Remote Sensing for Vegetation Monitoring

Satellite remote sensing has completely revolutionized the understanding of vegetation monitoring, focusing into vegetation health, growth trends, and ecological change. Specifically, the MODIS Vegetation Index (L3, 16-Day) layer provides a summary of vegetation conditions every 16 days at a

250-m spatial resolution, which is very beneficial in the field of vegetation dynamic monitoring [9]. A key parameter derived from MODIS is the NDVI, which calculates the difference between near-infrared light, highly reflected by vegetation, and visible red light, which vegetation strongly absorbs. NDVI is calculated by:

$$\text{NDVI} = \left(\frac{NIR - RED}{NIR + RED}\right) \quad (1)$$

where *NIR* is the reflectance of near-infrared light (typically around 0.76-0.90 μm) and *RED* is the reflectance of visible red light (typically around 0.63-0.69 μm). *NDVI* values range from -1 to +1, with higher values indicating healthy, dense vegetation, while lower values representing less vegetation or non-vegetated surfaces.

Such data are particularly crucial for regions affected by prolonged droughts, which severely impact vegetation cover and ecosystem functioning [10-12]. For instance, authors in [13] utilized NDVI in monitoring drought conditions in sub-Saharan Africa, providing valuable early warnings for food security planning. Furthermore, the integration of these tools with land-use strategies enables researchers and policymakers to track vegetation trends, assess ecosystem health, and mitigate the impacts of environmental degradation through informed interventions. It has been shown that NDVI, along with indices, such as the Global Vegetation Moisture Index (GVMI) and the Normalized Difference Water Index (NDWI), serves as an important input for CNN-based ecological modeling [14]. For the last decade, MODIS NDVI data have revealed that, for most parts of northern Kazakhstan, a 5% increase in vegetation has occurred due to more frequent rains, while for southern Kazakhstan, a 7% decrease in vegetation growth has occurred due to drought [15].

The historical data obtained from the Advanced Very High-Resolution Radiometer (AVHRR) of the National Oceanic and Atmospheric Administration (NOAA) complements MODIS NDVI data by providing a long-term historical record dating back to the late 1970s [16]. While AVHRR offers long-term temporal coverage, MODIS ensures high-quality and precise helping the tracking of vegetation changes influenced by environmental factors. The MODIS algorithm, as illustrated in Figure 3, identifies the optimal possible pixel values by selecting those with minimal cloud cover, optimum viewing angles, and the highest *NDVI* values [17].

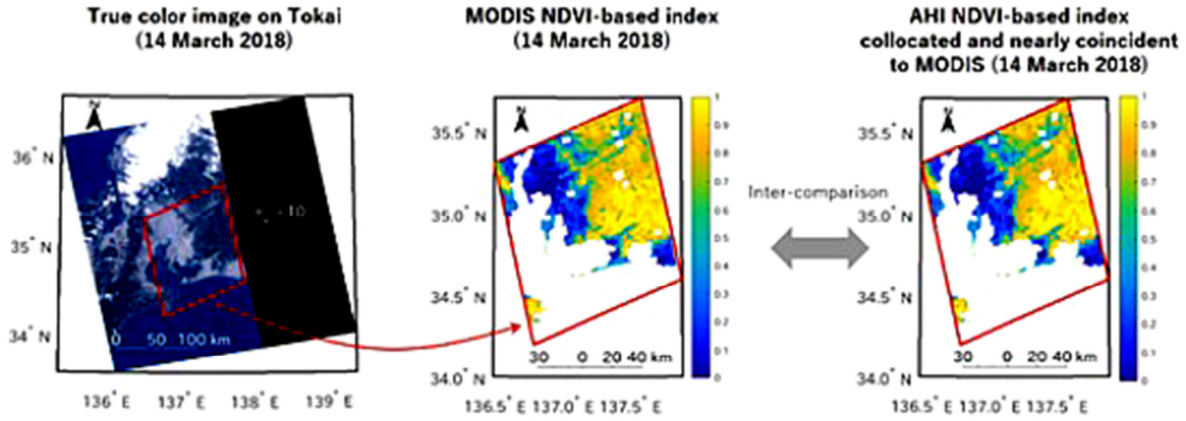

Fig. 3. Illustration of the MODIS target area extraction process and NDVI-based indices.

D. Gathering Satellite Data

Satellite data were collected through NASA's Worldview Snapshot API, a service that enables automated access to georeferenced Earth observation imagery. Python scripts were developed to streamline the data acquisition process, allowing the daily download of MODIS vegetation layers, reflectance products, and precipitation data. These scripts handled not only the API interaction, but also spatial filtering, date iteration, and storage management, ensuring reproducibility and scalability.

For preprocessing, tools such as NumPy and SciPy were utilized for normalization and filtering, while Geospatial Data Abstraction Library (GDAL) facilitated coordinate transformation and raster handling. Data were systematically organized by type, date, and spatial region to support efficient retrieval during model training and evaluation. Additionally, temporal metadata were employed to index and align the datasets.

This structured and automated approach enhanced data quality and enabled robust integration with downstream deep learning pipelines. A visual example of the dataset is presented in Figures 4 and 5. NDVI-based vegetation patterns over Kazakhstan derived from the MODIS Aqua L3 product are illustrated in Figure 4, while Figure 5 depicts the precipitation patterns, using a combination of data layers that include the MODIS Terra Corrected Reflectance True Color, AMSR2, and SSMI/DMSP instruments. These layers provided a comprehensive coverage of precipitation events, crucial for correlating vegetation health with water availability in these arid and semi-arid regions [18].

Figure 6 presents the vegetation cover (green shading) and precipitation distribution (blue shading) derived from satellite data, while Figure 7 illustrates the preprocessed vegetation distribution.

Fig. 4. Vegetation distribution of Kazakhstan covering the region bounded by the coordinates Top Right: (Latitude 55.5607, Longitude 87.5943) and Bottom Left: (Latitude 36.4112, Longitude 46.2757). NASA Worldview: https://worldview.earthdata.nasa.gov/.

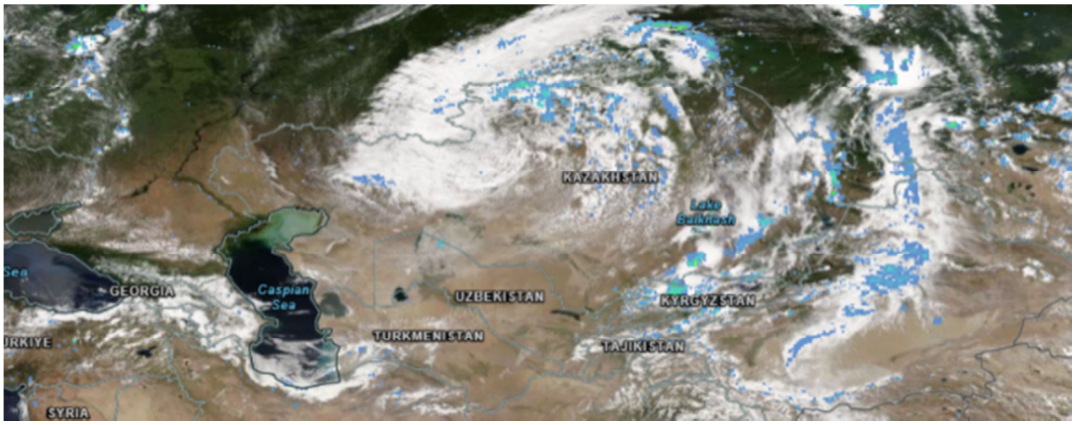

Fig. 5. Precipitation map of Kazakhstan covering the region bounded by the coordinates Top Right: (Latitude 55.5607, Longitude 87.5943) and Bottom Left: (Latitude 36.4112, Longitude 46.2757).). NASA Worldview: https://worldview.earthdata.nasa.gov/.

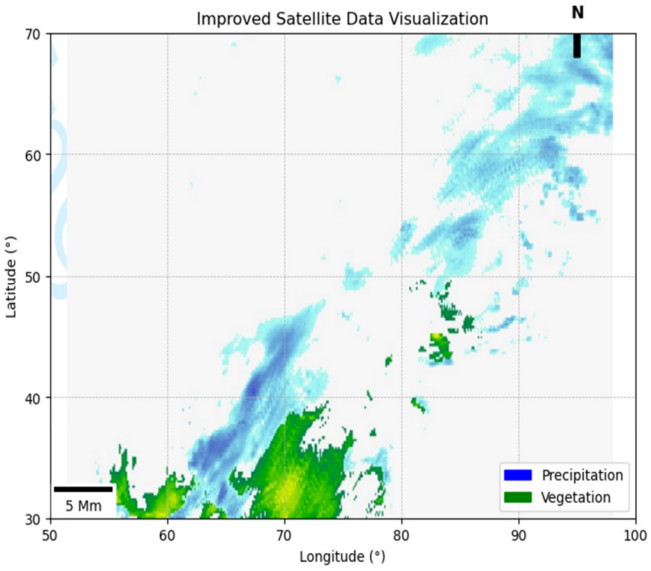

Fig. 6. Improved satellite-based visualization of vegetation and precipitation patterns across Kazakhstan.

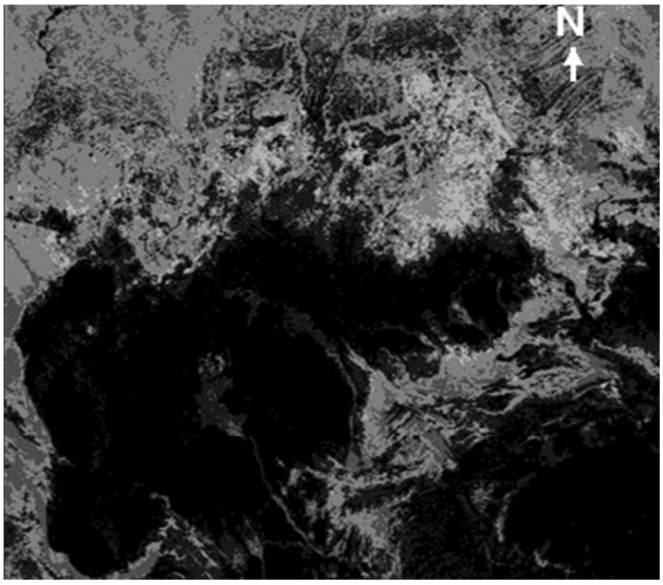

Fig. 7. Gathered and preprocessed vegetation image.

E. Preprocessing Techniques

Distinct preprocessing approaches were implemented for vegetation and precipitation data to optimize them for deep-learning applications. Specifically, they focused on analyzing and predicting vegetation dynamics, which referred to changes in vegetation health, density, and distribution over time and space in response to environmental factors, such as climate variability, precipitation patterns, and human activities.

For vegetation analysis, satellite data were captured almost daily by MODIS, but the NDVI product was derived from 16-day composites. These composites provided a more stable view of the vegetation cover over time, as daily reflectance images, which are acquired more frequently, may contain redundant information for this particular analysis. To streamline the model's performance and focus on the key features, the NDVI data were converted to a single channel format, which merged multiple channels representing different reflectance dynamics into one grayscale image (Figure 8). This simplification reduced computational complexity without losing critical information. The images were stored in the PyTorch tensor format ('*.pt'), which maintained data integrity for further analysis.

On the other hand, precipitation data presented unique challenges due to their daily variability and the distinct effects of different precipitation types, such as rain and snow, on vegetation. To address these challenges, precipitation data for each 16-day vegetation monitoring period were aggregated into a composite file. Each day was represented by three channels corresponding to rainfall, snowfall, and mixed precipitation, resulting in a total of 48 channels (16 days × 3 channels). This structure allowed the model to differentiate the varying impacts of precipitation types on vegetation dynamics.

The original resolution of these data (2,048 × 4,096 pixels) was resized to 512 × 512 pixels. Each pixel represented an aggregated value derived from the corresponding area in the original image, ensuring the spatial integrity of the data while reducing computational demands. This resizing process helped streamline the model training pipeline without compromising the quality and detail required for accurate predictions. As described in Figure 8, the pipeline was designed to optimize the input data for deep learning models, enhancing the model's prediction ability. By structuring the data effectively and tailoring the preprocessing steps to the needs of the study, the research demonstrated the utility of advanced ML techniques [19] for analyzing vegetation dynamics in Kazakhstan.

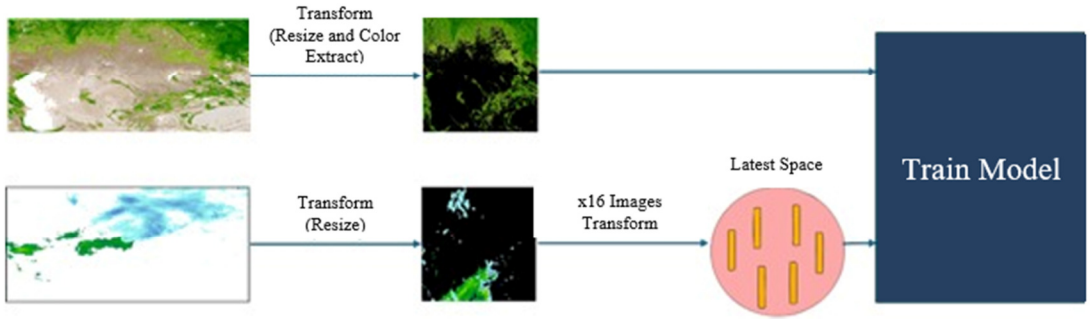

Fig. 8. Dataset creation end-to-end pipeline.

III. MODEL BUILDING AND ANALYSIS

The accurate prediction of vegetation dynamics required a modeling approach capable of capturing both the spatial and temporal complexities inherent in ecological data. To achieve this, a hybrid deep learning model was developed, integrating CNNs and RNNs. CNNs are well-suited for extracting spatial features from satellite imagery, identifying intricate patterns, and variations in vegetation cover, while RNNs -particularly LSTMs- capture temporal dependencies, enabling analysis of vegetation changes over time and predictions of future states [20].

The model was designed to address challenges associated with high-dimensional ecological data, such as computational efficiency, prevention of overfitting, and scalability. By incorporating advanced systems, like batch normalization, dropout, and gradient clipping, the architecture ensured stability during training while maintaining high predictive accuracy and practical applicability [21].

A. Model Architecture

The proposed deep learning architecture was created to analyze and predict vegetation dynamics from satellite imagery, containing convolutional, pooling, and fully connected layers. Specifically, convolutional layers can automatically extract spatial structures in images, detecting vegetation changes [22]. MaxPooling layers reduce feature map size while preserving essential information [23] and fully connected layers process the extracted features, with batch normalization and dropout be applied to stabilize training and prevent overfitting.

To capture temporal dependencies efficiently, Gated Recurrent Units (GRUs) were utilized, simplifying the architecture and reducing computational complexity compared to LSTMs, which predict vegetation changes by analyzing time-series satellite imagery [24, 25].

The model processed input images of size 512 × 512 × 3 (Table I). A series of convolutional layers increased the number of filters from 32 to 512, alternated with MaxPooling layers to reduce dimensionality. The final convolutional output was

passed to an Adaptive Average Pooling layer (AdaptiveAvgPool2d), preparing it for the fully connected layers. These by turn, contained a significant number of parameters with the first one having 134 million, the second 4 million, and the last 268 million. In total, the model involved 408 million parameters and consumed 1,770 MB of memory.

Visualization techniques for CNNs helped interpret extracted features and optimize the model architecture [25, 26]. Model improvements can be achieved by reducing the number of parameters in the fully connected layers and eliminating redundant computations.

Following the initial layer, the model employed a deeper convolutional layer (Conv2d-2) (Figure 9), with 32 channels and 896 parameters, allowing for more complex feature extraction without a substantial rise in computational cost [27].

TABLE I. COMPLETE MODEL ARCHITECTURE

Layer (Type)	Output shape	Parameters
Conv2d-1	-1, 3, 512, 512	147
Conv2d-2	-1, 32, 512, 512	896
MaxPool2d-3	-1, 32, 256, 256	0
Conv2d-4	-1, 64, 256, 256	18,496
MaxPool2d-5	-1, 64, 128, 128	0
Conv2d-6	-1, 128, 128, 128	73,856
MaxPool2d-7	-1, 128, 64, 64	0
Conv2d-8	-1, 256, 64, 64	295,168
MaxPool2d-9	-1, 256, 32, 32	0
Conv2d-10	-1, 512, 32, 32	1,180,160
MaxPool2d-11	-1, 512, 16, 16	0
AdaptiveAvgPool2d-12	-1, 512, 8, 8	0
Linear-13	-1, 4096	134,221,824
Linear-14	-1, 1024	4,195,328
Linear-15	-1, 262,144	268,697,600
Total parameters	-	408,683,475

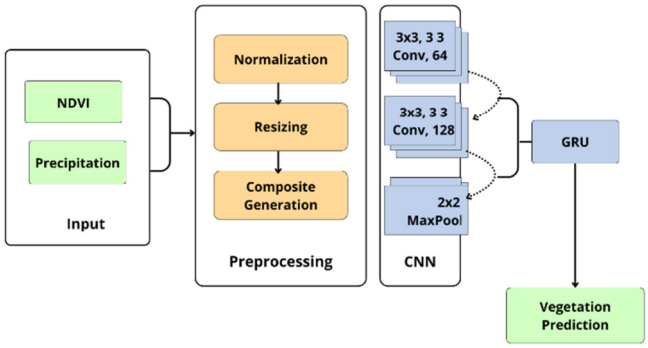

Fig. 9. Convolution layer in model architecture.

B. Model Training and Optimization

The model's efficiency relied not only on its architecture, but also on its training and optimization. Advanced methods, including adaptive optimizers, regularization, and gradient stabilization, ensured reliable analysis and prediction of vegetation dynamics.

During training, NDVI and EVI indices were processed through CNNs and RNNs. The model adjusted its parameters using the Adam optimizer, which combined Momentum and Root Mean Square Propagation (RMSProp) to efficiently manage sparse gradients and improve convergence speed by over 50% compared to traditional methods [28].

Additionally, techniques, such as batch normalization, dropout, and regularization prevented overfitting. Generally, batch normalization accelerates training, stabilizes learning, and reduces the number of required epochs by 20% [29], while dropout prevents overfitting by deactivating random neurons, improving generalization by about 4%. Parallel computing resources, like GPUs and TPUs, significantly speeded up training, supporting large-scale ecological data processing. Learning rate decay and early stopping strategies improved efficiency by up to 10% in deep architectures [30]. In these experiments, an optimal learning rate of 0.001 was identified using validation loss-based early stopping. Gradient clipping was also implemented to ensure stable weight updates and preventing divergence [31].

IV. RESULTS AND DISCUSSION

Developing effective predictive models for vegetation dynamics involves handling the complexities of large neural networks. In this study, the application of ResNet-50, a model well-known for its depth and complexity with few parameters was initially considered [32]. This model was first designed for classification, containing around 23 million parameters and 50 convolutional layers [33]. Despite its sophisticated architecture, the model's performance in this investigation was suboptimal, as detailed in Figure 10, which depicts the poor results obtained from initial tests. This inefficacy could be attributed to several factors intrinsic to the nature of the specific application.

(a)

(b)

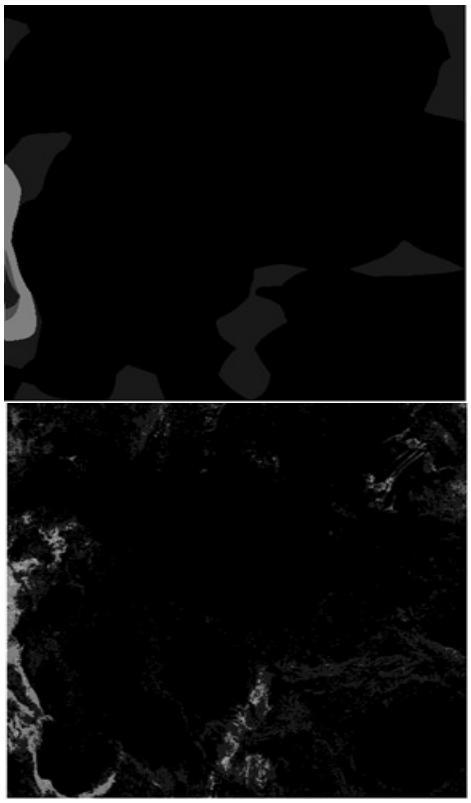

Fig. 10. (a) ResNet-50 Model and (b) actual image of vegetation.

The pixel-level prediction required for vegetation health and coverage did not aligned well with the classification strengths of ResNet-50. An attempt to classify pixel data into five distinct classes was developed within specific intervals: [0, 0.1, 0.3, 0.5, 0.7]. This classification was designed to handle the prevalence of black pixels (0 value), which are common in satellite imagery due to shadowing and other factors, by assigning them to a distinct class. Figure 11 illustrates the architecture of the ResNet50 model used in this experiment, detailing its complex structure and numerous layers.

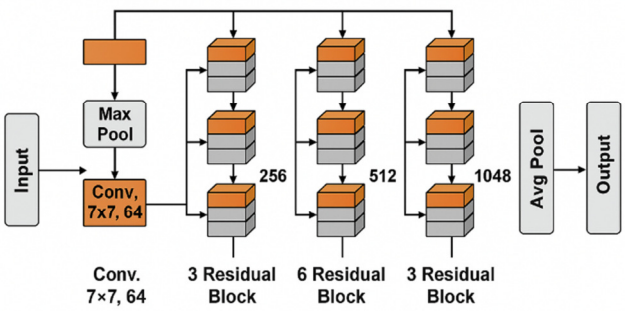

Fig. 11. Architecture of ResNet50 model used for vegetation dynamics prediction.

The confusion matrix of this model is presented in Table II. While its accuracy was recorded at 86.7%, this metric was not appropriate given the class imbalance in the dataset. As a result, the balanced-accuracy score significantly dropped to 61.2%. To address the complexity and overfitting risks associated with deep models, dropout, batch normalization, and custom loss functions were incorporated during training. These enhancements improved the model's generalization ability and robustness when applied to unseen data. Specifically, dropout helped prevent co-adaptation of neurons, batch normalization stabilized the learning process, and task-specific loss functions ensured more meaningful gradient updates in the context of vegetation regression.

TABLE II. CONFUSION MATRIX FOR RESNET-50 MODEL

	Predicted	**Predicted 1**	**Predicted 2**	**Predicted 3**	**Predicted 4**
Class 0	217012	812	663	454	546
Class 1	15750	7812	3023	5012	3626
Class 2	1099	300	1012	1032	1111
Class 3	209	215	312	1533	512
Class 4	1	3	15	22	58

Figure 12 presents the convergence of training and testing loss across 30 epochs, demonstrating the effective learning rate of 0.0001, which was selected based on optimization studies, as shown in Table III. The regression model, utilizing a sequence of deep learning architectures, demonstrated remarkable performance in terms of loss reduction and prediction accuracy over the training period. Specifically, the model learned to predict vegetation dynamics based on temporal and spatial features, effectively capturing critical trends and relationships within the dataset. This was evidenced by the training and testing loss data:

- Epoch 1/30, Train Loss: 0.0419, Test Loss: 0.0160
- Epoch 30/30, Train Loss: 0.0055, Test Loss: 0.0091

In Table IV, various learning rates were compared along with their impact on the speed and stability of convergence, establishing that a rate of 0.0001 provided the optimal balance for the current model. Table V further detailed the training and testing loss for the best hyperparameters, confirming the model's stability and generalization performance. In addition to quantitative metrics, visual results also played a pivotal role in evaluating model performance. Particularly, predicted grayscale images of vegetation health (Figure 13), revealed critical spatial patterns and temporal dynamics in vegetation conditions. By comparing these images with the original ground descriptions (Figure 14), the accuracy and performance of this model can be determined. The findings of this comparison demonstrated that the model was not merely reproducing the input images but instead it generated meaningful predictions based on learned representations of vegetation dynamics from the input data.

To verify the significance of these results, a comparison between the proposed model and the results of previous studies in the field of vegetation forecasting was developed. For instance, authors in [6] investigated the utility of autoencoders for tabular data classification in ecological tasks but did not incorporate spatial structures or raw satellite imagery. In contrast, this approach utilized raw NDVI composites and synchronized precipitation maps, enabling pixel-level predictions with spatial context preserved. Authors in [22] employed LSTM networks to construct global NDVI and EVI time series, focusing primarily on temporal trends. While their work achieved strong performance in modeling temporal continuity, it lacked integration with auxiliary climatic variables, such as precipitation. Similarly, in [21], the use of RNNs was explored for forecasting environmental variables but did not apply these methods to the vegetation domain or integrate high-resolution remote sensing data. In contrast, the proposed method combined CNNs for spatial feature extraction and recurrent networks for temporal modeling, supported by a robust preprocessing pipeline. This hybrid architecture, along with the use of precipitation composites from AMSR2, SSMI/DMSP, and IMERG sources, achieved high accuracy (*MAE* = 0.0091) in predicting vegetation health, especially under the challenging conditions of arid and semi-arid regions.

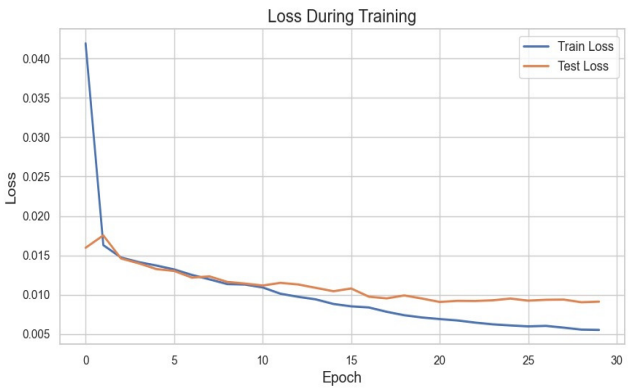

Fig. 12. Training and testing loss over epochs.

TABLE III. TRAIN/TRAINING DATASET LOSS FUNCTION SUM

Epoch learning rate	0.1	0.001	0.0001	0.00001
10	0.550	0.430	0.3110	0.450
20	0.470	0.390	0.3205	0.410
30	0.460	0.370	0.3102	0.400
40	0.445	0.360	0.3150	0.390
50	0.435	0.350	0.3170	0.380

TABLE IV. TEST DATASET LOSS FUNCTION SUM

Epoch learning rate	0.1	0.001	0.0001	0.00001
10	0.550	0.430	0.3110	0.450
20	0.470	0.390	0.3205	0.410
30	0.460	0.370	0.3102	0.400
40	0.445	0.360	0.3150	0.390
50	0.435	0.350	0.3170	0.380

TABLE V. TRAINING AND TESTING LOSS FOR BEST HYPERPARAMETERS

Epochs	Train loss	Test loss
1	0.0419	0.016
2	0.0163	0.0175
3	0.0147	0.0146
4	0.0141	0.014
5	0.0132	0.0132
6	0.0132	0.013
7	0.0124	0.0122
8	0.0119	0.0123
9	0.0113	0.0116
10	0.0113	00114
11	0.0109	0.0112
12	0.0107	0.0115
13	0.0101	0.0111
14	0.0094	0.0109
15	0.0094	0.0108
16	0.0085	0.0108
17	0.0080	0.0106
18	0.0074	0.0095
19	0.0073	0.0099
20	0.0071	0.0096
21	0.0069	0.0095
22	0.0067	0.0092
23	0.0064	0.0092
24	0.0062	0.0093
25	0.0061	0.0092
26	0.0060	0.0092
27	0.0060	0.0092
28	0.0058	0.0092
29	0.0056	0.009
30	0.0055	0.0091

V. CONCLUSIONS

This study examined the use of advanced deep learning approaches for predicting vegetation dynamics across a wide range of ecological zones in Kazakhstan. The integration of Convolutional Neural Networks (CNNs) and Recurrent Neural Networks (RNNs) proved to be effective in dealing with the time-series vegetation cover associated with satellite imaging and climate data. A methodological framework was prepared for inputting Moderate Resolution Imaging Spectroradiometer (MODIS)-derived indices, such as Normalized Difference Vegetation Index (NDVI) and Enhanced Vegetation Index (EVI), into these models, allowing effective assessment of vegetation changes over time. Model training and optimization were carried out through techniques, such as batch normalization and dropout together with the Adam optimizer.

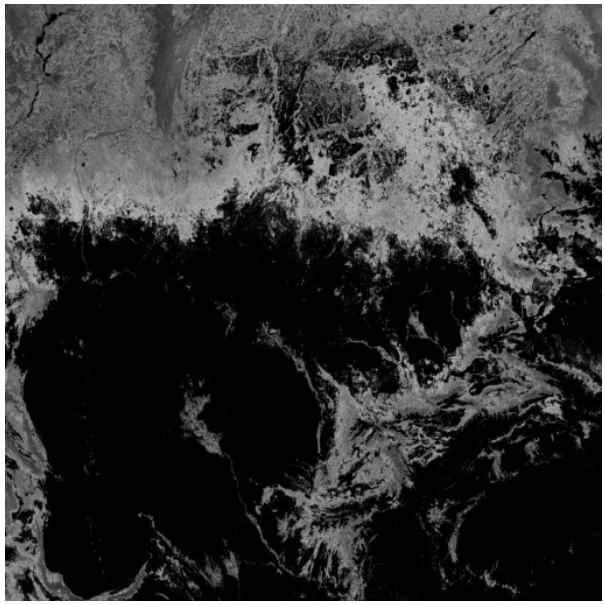

Fig. 13. Predicted grayscale map of vegetation health indicators, covering the region bounded by the coordinates. Top right: (latitude 55.5607, longitude 87.5943) and bottom left: (latitude 36.4112, longitude 46.2757).

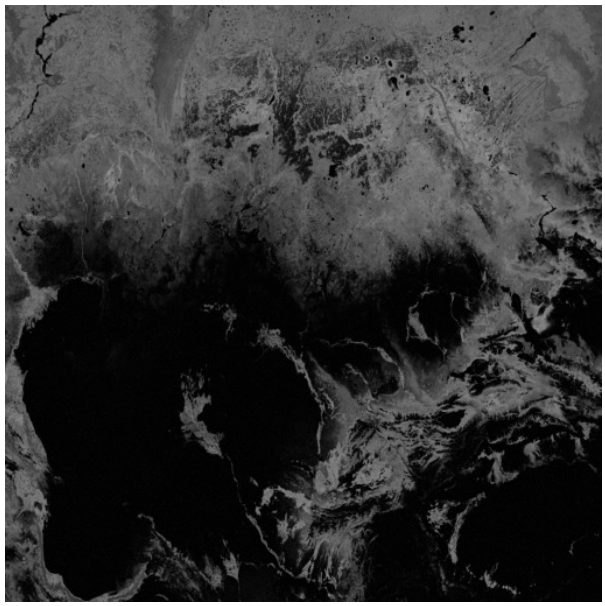

Fig. 14. Original ground truth grayscale map of vegetation health indicators, covering the region bounded by the coordinates. Top right: (latitude 55.5607, longitude 87.5943) and bottom left: (latitude 36.4112, longitude 46.2757).

An experimental application of ResNet50 for classification was considered, with the results demonstrating suboptimal observation compared to the actual data. Due to this, a reformulation of regression problem was vital, as well as the incorporation of dropout, batch normalization, and custom loss functions during training. The output of this reformation

indicated that deep learning was effective in predicting vegetation dynamics with very high accuracy. Model validations with different independent metrics allowed showing the engaging behavior to the real data of the predicted values of the models, thus providing real potential application (*MAE* = 0.0091).

Also, more complex models with advanced architectures, such as hybrid models combining CNNs with graph neural networks, could be introduced to handle even larger datasets with greater variability. This would, in turn, make predictions in different biomes even more accurate and provide for region-specific conservation strategies, ultimately expanding the applicability of ecological forecasting models on a global scale.

ACKNOWLEDGMENT

This research was supported by the Science Committee of the Ministry of Science and Higher Education of the Republic of Kazakhstan (Grant No. BR24992865).

REFERENCES

[1] "The Fifth National Report on Progress in Implementation of the Convention on Biological Diversity," Ministry of Environemtnal and Water Resources of the Republic of Kazakhstan, 2014.

[2] "Wildlife of Kazakhstan – Iconic Heritage of Future Generations." UNDP Kazakhstan, https://www.undp.org/kazakhstan/stories/wildlife-kazakhstan-iconic-heritage-future-generations.

[3] P. Micklin, "The Aral Sea Disaster," *Annual Review of Earth and Planetary Sciences*, vol. 35, pp. 47–72, May 2007, https://doi.org/10.1146/annurev.earth.35.031306.140120.

[4] S. L. O'Hara, G. F. Wiggs, B. Mamedov, G. Davidson, and R. B. Hubbard, "Exposure to airborne dust contaminated with pesticide in the Aral Sea region," *The Lancet*, vol. 355, no. 9204, pp. 627–628, Feb. 2000, https://doi.org/10.1016/S0140-6736(99)04753-4.

[5] "2022 Tied for Fifth Warmest Year on Record," *NASA Earth Observatory*, 2022, https://earthobservatory.nasa.gov/images/150828/2022-tied-for-fifth-warmest-year-on-record.

[6] A. Altaibek, I. Tokhtakhunov, M. Nurtas, D. Kozhamzharova, and M. Aitimov, "The Efficacy of Autoencoders in the Utilization of Tabular Data for Classification Tasks," *Procedia Computer Science*, vol. 238, pp. 492–502, Jan. 2024, https://doi.org/10.1016/j.procs.2024.06.052.

[7] A. Kairanbayeva *et al.*, "Predictive System for Road Condition Monitoring Based on Open Climate and Remote Sensing Data – A Case Study with Mountain Roads," *Engineered Science*, vol. 28, no. 2, Jan. 2024, Art. no. 1081, https://doi.org/10.30919/es1081.

[8] G. Esen, A. Altaibek, J. Amankulov, B. Matkerim, and M. Nurtas, Enhancing Breast Cancer Detection with Dimensionality Reduction Techniques: A Study Using PCA and LDA on Wisconsin Breast Cancer Data," *Procedia Computer Science*, vol. 251, pp. 414–421, Jan. 2024, https://doi.org/10.1016/j.procs.2024.11.128.

[9] K. Didan, A. B. Munoz, R. Solano, and A. Huete, "MODIS Vegetation Index User's Guide (MOD13 Series)." Vegetation Index and Phenology Lab, Jun. 2015, https://vip.arizona.edu/documents/MODIS/MODIS_VI_UsersGuide_June_2015_C6.pdf.

[10] C. J. Tucker, J. R. G. Townshend, and T. E. Goff, "African Land-Cover Classification Using Satellite Data," *Science*, vol. 227, no. 4685, pp. 369–375, Jan. 1985, https://doi.org/10.1126/science.227.4685.369.

[11] H. J. Geist and E. F. Lambin, "Proximate Causes and Underlying Driving Forces of Tropical Deforestation: Tropical forests are disappearing as the result of many pressures, both local and regional, acting in various combinations in different geographical locations," *BioScience*, vol. 52, no. 2, pp. 143–150, Feb. 2002, https://doi.org/10.1641/0006-3568(2002)052[0143:PCAUDF]2.0.CO;2.

[12] N. Pettorelli, J. O. Vik, A. Mysterud, J.-M. Gaillard, C. J. Tucker, and N. C. Stenseth, "Using the satellite-derived NDVI to assess ecological responses to environmental change," *Trends in Ecology & Evolution*, vol. 20, no. 9, pp. 503–510, Sep. 2005, https://doi.org/10.1016/j.tree.2005.05.011.

[13] C. J. Tucker, C. Vanpraet, E. Boerwinkel, and A. Gaston, "Satellite remote sensing of total dry matter production in the Senegalese Sahel," *Remote Sensing of Environment*, vol. 13, no. 6, pp. 461–474, Dec. 1983, https://doi.org/10.1016/0034-4257(83)90053-6.

[14] E. H. Hegazi, A. A. Samak, L. Yang, R. Huang, and J. Huang, "Prediction of Soil Moisture Content from Sentinel-2 Images Using Convolutional Neural Network (CNN)," *Agronomy*, vol. 13, no. 3, Mar. 2023, Art. no. 656, https://doi.org/10.3390/agronomy13030656.

[15] R. F. Sage, "Global change biology: A primer," *Global Change Biology*, vol. 26, no. 1, pp. 3–30, 2020, https://doi.org/10.1111/gcb.14893.

[16] F. Baret *et al.*, "VALERI: a network of sites and a methodology for the validation of medium spatial resolution land satellite products," *Remote Sensing of Environment*, vol. 76, no. 3, pp. 36–39, 2005.

[17] H. Xu, Y. Wang, H. Guan, T. Shi, and X. Hu, "Detecting Ecological Changes with a Remote Sensing Based Ecological Index (RSEI) Produced Time Series and Change Vector Analysis," *Remote Sensing*, vol. 11, no. 20, Jan. 2019, Art. no. 2345, https://doi.org/10.3390/rs11202345.

[18] A. Altaibek, M. Nurtas, Z. Zhantayev, B. Zhumabayev, and A. Kumarkhanova, "Classifying Seismic Events Linked to Solar Activity: A Retrospective LSTM Approach Using Proton Density," *Atmosphere*, vol. 15, no. 11, Nov. 2024, Art. no. 1290, https://doi.org/10.3390/atmos15111290.

[19] M. Pritt and G. Chern, "Satellite Image Classification with Deep Learning," in *2017 IEEE Applied Imagery Pattern Recognition Workshop (AIPR)*, Washington, DC, USA, Oct. 2017, pp. 1–7, https://doi.org/10.1109/AIPR.2017.8457969.

[20] Z. Ao, Y. Sun, and Q. Xin, "Constructing 10-m NDVI Time Series From Landsat 8 and Sentinel 2 Images Using Convolutional Neural Networks," *IEEE Geoscience and Remote Sensing Letters*, vol. 18, no. 8, pp. 1461–1465, Aug. 2021, https://doi.org/10.1109/LGRS.2020.3003322.

[21] Y. Chen, Q. Cheng, Y. Cheng, H. Yang, and H. Yu, "Applications of Recurrent Neural Networks in Environmental Factor Forecasting: A Review," *Neural Computation*, vol. 30, no. 11, pp. 2855–2881, Nov. 2018, https://doi.org/10.1162/neco_a_01134.

[22] C. Xiong *et al.*, "Improved global 250 m 8-day NDVI and EVI products from 2000–2021 using the LSTM model," *Scientific Data*, vol. 10, no. 1, Nov. 2023, Art. no. 800, https://doi.org/10.1038/s41597-023-02695-x.

[23] Y. LeCun, Y. Bengio, and G. Hinton, "Deep learning," *Nature*, vol. 521, no. 7553, pp. 436–444, May 2015, https://doi.org/10.1038/nature14539.

[24] L. P. Osco *et al.*, "A review on deep learning in UAV remote sensing," *International Journal of Applied Earth Observation and Geoinformation*, vol. 102, Oct. 2021, Art. no. 102456, https://doi.org/10.1016/j.jag.2021.102456.

[25] S. Ruder, "An overview of gradient descent optimization algorithms." arXiv, Jun. 15, 2017, https://doi.org/10.48550/arXiv.1609.04747.

[26] M. D. Zeiler and R. Fergus, "Visualizing and Understanding Convolutional Networks," in *13th European Conference*, Zurich, Switzerland, 2014, pp. 818–833, https://doi.org/10.1007/978-3-319-10590-1_53.

[27] K. Simonyan and A. Zisserman, "Very Deep Convolutional Networks for Large-Scale Image Recognition." in *3rd International Conference for Learning Representations*, San Diego, CA, USA, 2015.

[28] D. P. Kingma and J. Ba, "Adam: A Method for Stochastic Optimization," in *3rd International Conference for Learning Representations*, San Diego, CA, USA, 2015.

[29] S. Ioffe and C. Szegedy, "Batch Normalization: Accelerating Deep Network Training by Reducing Internal Covariate Shift," in *Proceedings of the 32nd International Conference on Machine Learning*, Lille, France, Jul. 2015, pp. 448–456, https://proceedings.mlr.press/v37/ioffe15.html.

[30] I. Loshchilov and F. Hutter, "SGDR: Stochastic Gradient Descent with Warm Restarts," in *5th International Conference on Learning Representations*, Toulon, France, 2017.

[31] R. Pascanu, T. Mikolov, and Y. Bengio, "On the difficulty of training recurrent neural networks," in *30th International Conference on Machine Learning*, Atlanta, GA, USA, May 2013, pp. 1310–1318.

[32] S. Mascarenhas and M. Agarwal, "A comparison between VGG16, VGG19 and ResNet50 architecture frameworks for Image Classification," in *2021 International Conference on Disruptive Technologies for Multi-Disciplinary Research and Applications (CENTCON)*, Bengaluru, India, Aug. 2021, vol. 1, pp. 96–99, https://doi.org/10.1109/CENTCON52345.2021.9687944.

[33] K. He, X. Zhang, S. Ren, and J. Sun, "Deep Residual Learning for Image Recognition," in *IEEE Conference on Computer Vision and Pattern Recognition*, Las Vegas, NV, USA, 2016, pp. 770–778.